JOURNAL OF AIRCRAFT
Vol. 45, No. 6, November–December 2008

High-Lift Devices Performance Enhancement Using Mechanical and Air-Jet Vortex Generators

M. Meunier* and V. Brunet†
ONERA, 92190 Meudon, France

DOI: 10.2514/1.36836

A growing number of advanced-research studies have recently examined the benefits of applying mechanical or fluidic separation control to leading-edge slats or trailing-edge flaps for high-lift geometries. In particular, the use of various control devices placed near the leading edge of a slotted flap mounted on a realistic three-element wing was successfully demonstrated in ONERA's F1 wind tunnel (Le Fauga-Mauzac Center), in the scope of the Advanced Aerodynamic Flow Control Using Microelectromechanical Systems II European project. The present paper aims at assessing the prediction accuracy of steady computational fluid dynamics simulations for flow-control problems, through a detailed validation procedure and comparisons against pressure measurements and skin-friction patterns obtained during the aforementioned experiment. In all, very good agreement was observed between numerical and wind-tunnel results, thus demonstrating the capability of Reynolds-averaged Navier–Stokes solvers to accurately predict such multiscale cases and the encouraging efficiency of conventional and modern actuators in strong adverse pressure gradients.

Nomenclature

C	=	chord
C_l	=	lift coefficient
C_p	=	pressure coefficient
C_μ	=	jet momentum coefficient
D	=	jet diameter
i	=	total quantity
L/D	=	lift-to-drag ratio
l_{ref}	=	reference length
M	=	Mach number
P	=	pressure
Q	=	normalized Q criterion = (vorticity^2-$\lvert S_{ij}\rvert^2$)
Re_l	=	l_{ref}-based Reynolds number
U	=	velocity
X	=	abscissa
y^+	=	normalized first cell height
α	=	angle of attack
δ	=	boundary-layer height
ρ	=	density
ω_x	=	normalized streamwise vorticity

Subscripts

flap	=	relative to the flap
j	=	relative to the jet
max	=	maximum value
∞	=	freestream quantity

I. Introduction

THE design of civil aircraft has undergone little evolution in the past two to three decades and remains predominantly oriented toward the attractive objective of steady wall streamlines, where separation is regarded as a highly penalizing phenomenon. Consequently, definition processes for modern wing plans appear to be somehow restricted to well-known and largely optimized configurations, so much so that the remaining aerodynamic improvements that are still achievable tend to be quite limited, at least in the current state of things.

In this context, flow control is unanimously regarded as a key evolution, offering new solutions for the performance maximization of existing designs and, to an even greater extent, the apprehension of new concepts, where separation management could be used in a multidisciplinary approach, fully integrated to the initial screening and conception phases. Technology is becoming more and more mature, in terms of power consumption [wide spreading of microelectromechanical systems (MEMS) technologies encompassed in periodic jets, or plasmas, for instance] and size integration, for industrial applications to be conceived and tested [1].‡

Among the most promising applications identified is the enhancement of severely loaded, trailing-edge flaps on high-lift airfoils, where boundary-layer separation is often encountered. Applying flow control to such cases could not only improve takeoff lift-to-drag ratio and landing maximum lift, but could also result in drastic reductions in radiated noise, mechanical complexity, weight, and manufacturing costs from simplifications and/or size reductions relative to current systems [2]. Besides several conclusive in-flight demonstrations [3–5] and a limited number of computational surveys, the aforementioned problem has been tackled mostly in wind-tunnel tests, implementing various actuating technologies, such as the following:

1) Conventional, passive, macro- and sub-boundary-layer vortex generators (SBVGs [6], Fig. 1) remain the easiest, safest, and cheapest solution for practical implementation in the near future. Simply deflected flat vanes, having a height on the order of a fifth of the local boundary-layer thickness, are placed slightly upstream of the separation point. They generate co- or counter-rotating streamwise vortices, which ensures a proper homogenization of the boundary-layer kinetic energy by momentum transfer from the outer to the inner regions.

In a series of publications, Lin et al. [7,8] and Klausmeyer et al. [9] reported on their investigations to evaluate boundary-layer separation control from a two-dimensional, three-element airfoil at near-flight Reynolds number with small surface-mounted vortex generators (VGs). They provide the reader with a large collection of

Received 25 January 2008; revision received 13 March 2008; accepted for publication 18 March 2008. Copyright © 2008 by the authors. Published by the American Institute of Aeronautics and Astronautics, Inc., with permission. Copies of this paper may be made for personal or internal use, on condition that the copier pay the $10.00 per-copy fee to the Copyright Clearance Center, Inc., 222 Rosewood Drive, Danvers, MA 01923; include the code 0021-8669/08 $10.00 in correspondence with the CCC.

*Aerospace Engineer, Applied Aerodynamics Department; mickael.meunier@onera.fr.

†Aerospace Engineer, Applied Aerodynamics Department; vincent.brunet@onera.fr.

‡Kral, L. D., "Active Flow Control Technology," ASME Fluids Engineering Division Technical Brief (Year of Publication Unknown); http://divisions.asme.org/fed/newsletter/TechBriefKral.pdf.

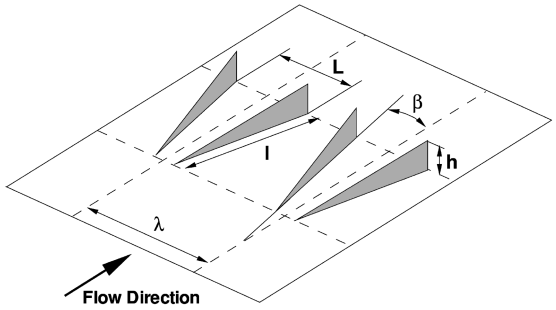

Fig. 1 Counter-rotating, trapezoidal vane vortex generators and associated defining parameters.

force, pressure, boundary-layer, laser Doppler velocimetry, as well as vortex strength and positioning measurements, eventually concluding that the apparent promise of micro-VGs suggests that they should be included directly within the design stages of an aircraft, rather than as after-design, curative, add-ons. Dodbele et al. [10] experimentally and computationally evaluated the aerodynamic performance of thin, fighter-type, multi-element airfoils having simple-hinged slats. Effects of Reynolds number, flap positioning, surface-mounted Gurney flaps, and vortex generators on $C_{l,\max}$ were investigated at flight conditions. Some Navier–Stokes computations were also found to be in good agreement with the experimental measurements. In the context of the Aircraft Wing with Advanced Technology Operation (AWIATOR) project, Rae et al. [11] successfully demonstrated the effects of SBVGs on complex, three-dimensional, trailing-edge flap separation, at a wide range of Reynolds numbers, suggesting that a full optimization of the actuated flap should be considered for performance maximization. Besides lift improvements, the removal of flow separation was shown to reduce buffet and flap performance sensitivity to gap settings. The authors conclude by analyzing the potential benefits and drawbacks (on aerodynamics, structural as well as industrial point of views) of applying VGs to current and future aircraft, yet quoting remaining uncertainties about sizing considerations.

Active, air-jet vortex generators (AJVGs [12], Fig. 2) consist of a small, pitched and skewed, continuously blowing jet, emerging from an aerodynamic surface relative to an oncoming upstream flow. Several jets arranged in a spanwise array generate longitudinal vortices similar to those of vane VGs. In contrast with the latter, AJVGs are known to offer improved penetration of the vortices (because they also benefit from jet entrainment effects [13]) combined with the advantage of very limited parasite skin-friction drag.

Innes et al. [14] used rectangular orifice, corotating jets mounted on the main body (at approximately 25% of the chord) of a three-element, two-dimensional configuration. They measured tremendous lift augmentations over the whole angle-of-attack range and a delay of up to 7.5 deg in maximum lift incidence when compared with the baseline case (whereas similarly placed vane VGs "only" delayed stall occurrence by 4.5 deg, with no lift increase reported at other angles of attack). The authors suggested that, besides the reattachment of the boundary layer, the AJVGs were responsible for an enhanced mixing and momentum transfer across the complex shear layers above the main element; a theory consistent with the findings of Lindblad and de Cock [15]. Lewington et al. [16,17] repeated the experiment using a computational fluid dynamics (CFD) based, interactive design procedure. The computational results provided the authors with useful guidelines, eventually resulting in a 6 deg stall delay and an increase of 25% in normal force coefficient relative to the uncontrolled scenario. As a part of the Advanced Aerodynamic Flow Control Using Microelectromechanical Systems (AEROMEMS) II program [18], Crowther [19] used flow control to loosen flap positioning tolerances while retaining constant overall performances. A swept high-lift model with an augmented flap gap (resulting in a net drop of 0.2 in C_l relative to the baseline geometry, for representative angles of attack) was equipped with an array of AJVGs, placed near the flap leading edge and blowing at a jet to local velocity ratio (VR) of VR = 2.6. Lift and pressure measurements demonstrated that the boundary layer could be reattached and original performance recovered, even with increased flap deflections. For an A320 type of aircraft, the author provides a provisional scaling in terms of mass flow requirements and concludes on a 0.5% engine mass flow bypass (based on a VR similarity parameter) for a constant jet exit velocity.

The introduction of unsteadiness in blowing jets for flow control has been an intense field of research in the last two decades and represents the best compromise between global efficiency and reasonable power or mass flow consumption(s). Two main designs were proposed throughout the years, namely, pulsed and synthetic jets [20]. The former is a derivative of continuous blowing jets, where an unsteady component is superimposed to the constant exiting mass flow, resulting in nonzero average momentum and mass flux characteristics. As a result, an external source of air is still required. The latter, on the other hand, uses the properties of resonating cavities and vibrating piezoelectric (or MEMS) membranes to produce the requested oscillations, with no need for external bleeding and limited power requirements. The result is a net positive momentum balance with a zero average exit mass flow. Whereas conventional and air-jet vortex generators rely on well-established streamwise vortices to enhance boundary-layer mixing, periodic jets also use mixing layer [21] concepts to generate large, coherent structures which are convected downstream and interact with the separating shear-layer instabilities. The physical mechanisms of the phenomenon remain to be fully understood but the results are very similar to those of AJVGs with momentum requests of 1 to 2 orders of magnitude less. The amount of literature available on the topic has grown exponentially in the last years and will not be discussed in details here. As far as high-lift applications are concerned, the detailed experiments by Seifert et al. [22–24], Nishri and Wygnanski [25], Tinapp and Nitsche [26,27], Petz and Nitsche [28,29], Schatz et al. [30], or Greenblatt [31], to name a few, are particularly interesting in that they demonstrate recurrent and persuasive conclusions (especially in terms of scaling parameters, i.e., blowing frequency C_μ and VR, although these are largely being discussed as similarity coefficients [32]) at widespread flight conditions and for extremely different, sometimes innovative, designs (see, for instance, the work by Pack Melton et al. [33–35], Kiedaisch et al. [36], or Becker et al. [37]).

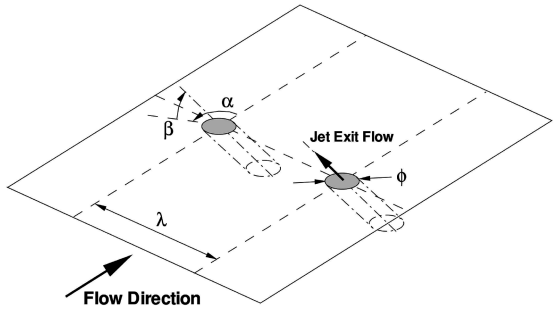

Fig. 2 Circular orifice, corotating air-jet vortex generators and associated defining parameters.

II. Objectives and Numerical Procedure

Computationally, the whole challenge of such configurations lies in the wide range of physical scales encountered, where the space discretization should be fine enough to capture the actuator-generated eddies, while remaining sufficiently coarse for industrial computations to be realistically considered and performed. The validation assessment procedure presented here started with the evaluation of an uncontrolled wing, followed by a demonstration of the effects of sub-boundary-layer vortex generators as well as continuous jets. In particular, a numerical model of a vane vortex generator was implemented and evaluated, which allows for a considerable reduction in grid sizes, much easier positioning and

parameterization of the control device, and the simulation of larger arrays of actuators.

The computational method used in this study relies on ONERA's structured, multiblock, cell-centered, elsA CFD software [38,39] [currently in industrial use within Airbus, Snecma, Turbomeca, Eurocopter, or MBDA (Matra British Aerospace Dynamics Alenia)]. The Reynolds-averaged form of the Navier–Stokes equations is solved using Jameson's second-order centered scheme with artificial viscosity for the spatial discretization. The implicit phase is resolved using a lower-upper symmetric successive overrelaxation technique, and convergence is accelerated through a one-level, v-cycle, multigrid algorithm combined with low-speed preconditioning. Turbulence closure is achieved under a Boussinesq hypothesis using the one-equation model of Spalart and Allmaras [40] (SA) or the two-equation k-ω formulation with Menter's shear stress transport (SST) correction [41]. Precise, fully turbulent, boundary-layer resolutions gave average y^+ values of approximately 0.2 and a maximum below 2 for all the meshes considered here.

Steady-state solutions were obtained using a quasi-stationary backward-Euler integration with a Courant–Friedrichs–Lewy-derived time step. For all cases, a thorough iterative convergence study (on residuals, forces, and moments) ensured that fully converged solutions were obtained.

To ensure that the simulation tool can be used as universally as possible in upcoming predictive studies involving flow-control applications, numerical settings commonly used in all conventional external aerodynamics computations were left entirely untouched, giving us a good idea of the degree of accuracy to be expected.

Fig. 3 AFV wing mounted in ONERA's F1 wind tunnel, showing the spanwise actuated flap section and the location of pressure measurement tapings.

III. Experimental Investigation: The AEROMEMS II High-Lift Tests

This study deals with a three-element airfoil that was tested in ONERA's F1 pressurized facility during the AEROMEMS II European project [18]. The aim was to bring an experimental demonstration, under industrial conditions, of separation control strategies for slotted flaps facing massively detached boundary layers. The experimental results presented here were reported by Flodrops [42], who detailed the experimental apparatus and calibration procedures for the constant blowing actuators.

The model that was used, the variable-sweep (AFV, French acronym) wing, is depicted in Fig. 3. It is a wall-mounted port half-wing, with a sweep angle of 40 deg, no taper or thickness changes from root to tip, and a half-span of 2 m. The two-dimensional wing section, taken normal to the leading edge, is based on a RA16SC1 design and has a nominal chord of 500 mm (main body, stowed flap). The slat deflection angle is set to 30 deg from the main body axis.

Tests in the frame of the EUROLIFT [43] campaign showed no traces of flow separation for a flap deflection angle of 40 deg over the freestream conditions considered. In a joint computational and experimental effort, modifications to the flap gap, overlap, and inclination were therefore applied (see Fig. 4), which ensured proper separation on the flap suction side. Because of compressed air supply and tubing issues, only a limited spanwise flap portion could be actuated and a single pressure measurement row retained. The control devices consisted of either corotating Laboratoire de Physique et Metrologie des Oscillateurs (LPMO) designed pulsed jets [44] (made to work continuously) or counter-rotating European Aeronautic Defence and Space Company (EADS) supplied SBVGs, both arrays being placed at 25% of the flap chord from the leading edge (LE).

Results for a unique freestream Mach number of $M_\infty = 0.22$ and Reynolds numbers of $Re_l = 3.13 \times 10^6$ (AJVGs, $U_\infty = 75.5$ m/s at $P_{i,\infty} = 1$ bar) and $Re_l = 6.27 \times 10^6$ (SBVGs, $U_\infty = 75.5$ m/s at $P_{i,\infty} = 2$ bar) will be presented herein. From the available pressure measurements, an experimental incidence of $\alpha_{3D} = 12$ deg was seen as the most representative of actuation effects and was chosen as a simulation reference.

IV. Results and Discussion

A. Meshing Strategy

Because of the variety of physical scales encountered, grid generation is of fundamental importance in flow-control problems. Previous in-house computations by Brunet et al. [45] for SBVGs on a flat plate have demonstrated that the need to precisely capture actuator-generated eddies produces computational domains of relatively important sizes, even for the simplest cases. This makes the computations of complete three-dimensional cases having multiple subscale devices practically impossible, at least industrially. It was therefore decided that all the simulations be run with an infinite wing hypothesis, using two-dimensional grids and periodic spanwise boundary conditions (hereafter referred to as 2.5-D computations). This is well suited to the AFV geometry which is known to behave almost entirely two-dimensionally at reasonable incidences [46].

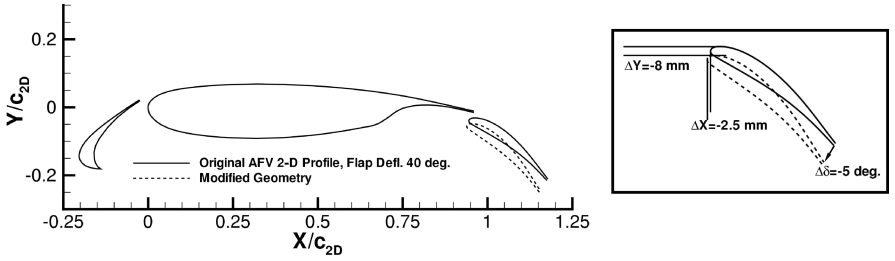

Fig. 4 AFV wing 2-D section and flap positioning modifications.

B. Results for the Uncontrolled Wing

To measure the influence of flap separation, and to quantify induced incidence effects (adaptation of the computational incidence to match the experimental slat and main-element peak loadings), the uncontrolled wing was rapidly assessed first at $Re_l = 3.13 \times 10^6$. A prismatic mesh was therefore created using the ANSYS-ICEM Hexa software. Having a C-O-H-type topology, it consists of approximately 100,000 points in a two-dimensional section, as seen in Fig. 5.

Figure 6 shows pressure distributions for the experimental and computational results, together with the resulting streamline arrangement over the flap. The effective incidence had to be corrected by -5 deg (a typical value for high-lift cases) to match three-dimensional effects. Note that the suction side measurement at $X/l_{\text{ref}} = 0.4$ corresponds to a faulty pressure tap, and should therefore not be accounted for in the following comparisons.

Results are seen to be in very good overall agreement with measurements, especially for the SA model (location of the separation line and constant pressure plateau). Only a slight discrepancy for the recirculation bubble sitting in the flap cove area is noticeable. Interestingly, the k-ω model could not reach a steady solution and seems to overestimate the size of the separated area, which in turn penalizes the accuracy of the main-element trailing-edge prediction. Transient simulations not reported here demonstrated no improvements to the solution and, although a single, low frequency dominated the spectrum, no vortex shedding was clearly identified, but rather a moderate instability in the streamwise location of the two contra-rotating eddies observed in Fig. 6 (in the absence of time-accurate pressure transducers, no reports can be made on the presence of large-scale unsteadiness in the experimental environment). Tests at other incidences showed that the flap pressure loading is almost independent of the angle of attack, which is a clear advantage for extended control authority.

As we intended to use the preceding mesh as a starting point for the upcoming controlled simulations (with only subsequent modifications to the actuator area), a thorough grid convergence study was conducted based on the SA model. Two low-level grids were therefore generated by applying a one-half (respectively, one-quarter) coarsening factor, in every direction, to the original mesh. The assessment methodology proposed by Roache [47] was then used as a quantifier for continuous extrapolation and convergence indexes, as illustrated in Fig. 7 and Table 1.

As a reminder, a unit ratio of grid convergence indexes (GCI) indicates asymptotic range of convergence. In terms of surface pressure, Fig. 8 depicts very limited differences between the fine and medium grid levels, even in the critical zones of the slat/main-element and main-element/flap-wake boundary-layer merging. The prediction of flap separation remains very robust indeed, indicative of a sufficient overall resolution. Although not discussed here, an analogous work was conducted for all the computations to be presented next, with similar conclusions.

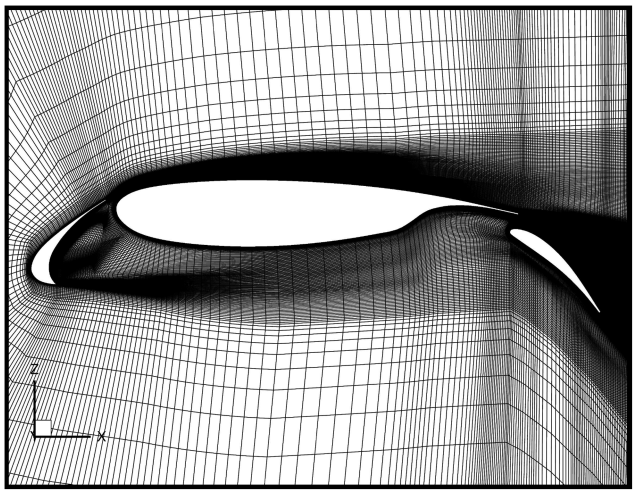

Fig. 5 Two-dimensional grid details and topology for the AFV wing, uncontrolled case.

C. Results for the 2.5-D Wing Equipped with Sub-Boundary-Layer Vortex Generators

1. Actuator Geometry and Mesh Specifications

The mechanical VGs used for the wind-tunnel test were designed by EADS Germany based on scaling recommendations by Godard and Stanislas [6]. Ten pairs of trapezoidal-shaped counter-rotating vanes (27 deg LE angle) were placed parallel to the flap LE at $X/c_{\text{flap}} = 25\%$ (slightly upstream of the separation point, for which

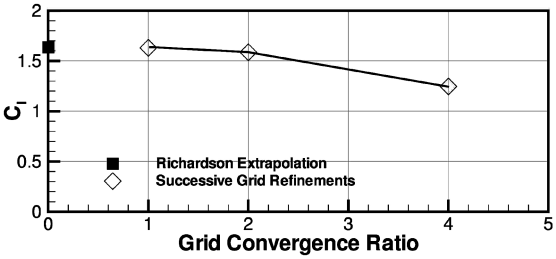

Fig. 7 Grid convergence assessment results for the uncontrolled case.

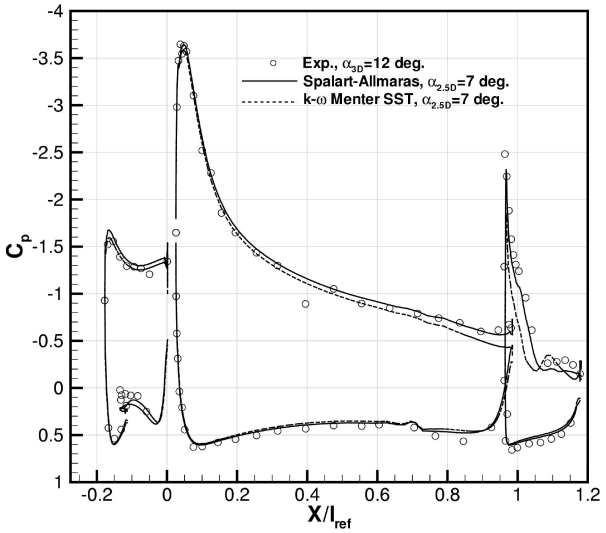

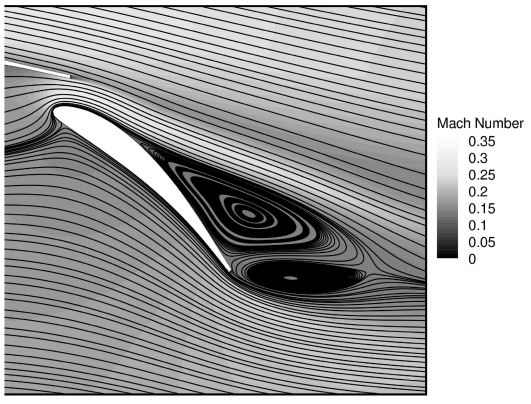

Fig. 6 Comparison of experimental and computational pressure distributions for the uncontrolled case, and corresponding flowfield.

Table 1 Grid convergence assessment results for the uncontrolled case

Mesh level	C_l
Fine	1.6298
Medium	1.5861
Coarse	1.2458
Richardson extrapolation	1.6362
Ratio of GCI	0.9732

$X/c_{\text{flap}} \approx 30$–$35\%$). Their dimensions, using the conventions defined in Fig. 1, are restated in Table 2 as a reminder.

The values given to these parameters emanate from preliminary boundary-layer computations, Fig. 9. To ensure that the VGs would have a realistic height and to retain a comfortable dimensioning margin, the wind-tunnel Reynolds number for this test case was also doubled to $Re_l = 6.27 \times 10^6$, giving a ratio of $h/\delta \approx 0.8$.

A unique pair of VGs was simulated. The original, uncontrolled grid was not modified in the slat, main-element, and far-field regions, with only the flap geometry being updated and meshed accordingly. Originally, the spanwise resolution depicted in Fig. 10 was extended to the entire computational domain, resulting in a mesh having around 23×10^6 nodes. To reduce the expected restitution time, a patched grid strategy [48] was therefore adopted. All the blocks outside the flap and flap-wake zones were coarsened using one-quarter partially coincident connections in the spanwise direction. The result is a savings of about 60% in the total number of grid points with a nominal mesh size of around 9×10^6 nodes.

2. *Results*

Figure 11 illustrates a comparison of experimental and computational surface pressures for the VG-controlled wing. The first thing to be noticed is that with an increased Reynolds number, the prediction of pressure levels in the separated region for the uncontrolled case does not seem to be as accurate as was previously demonstrated (possibly because of meshing effects, as a unique grid was used for all Reynolds numbers). The location of the separation point, however, is perfectly well evaluated. The effects of boundary-layer mixing from the actuators are also clearly visible and in very good agreement with experimental observations.

As seen in Fig. 12, the flow over the flap could be almost entirely reattached, with only a limited pressure plateau persisting. From the computational distributions, it would appear that the complete geometry benefits from a modified flow around the flap, with increased suction levels on the slat and main element. This can be explained by the fact that flap reattachment modifies the local trailing-edge downwash and, by linking effects through the slots, the circulation of the entire configuration. Experimental measurements, however, do not yield the same conclusions. Three-dimensional properties might therefore have to be accounted for and induced incidence effects recalibrated (need to decrease the two-dimensional angle of attack by 1–2 deg), as latter computations will demonstrate.

Table 2 Design parameters for the SBVGs

h	0.8 mm
l	3.6 mm
L	4.5 mm
λ	10.8 mm
β	18 deg

When looking at Fig. 13, we can make several further comments. First, from the plot of isosurfaces of Q criterion, it is evident that a strong nonequilibrium exists in the sizes of the structures generated by each pair. The positioning and configuration of the actuators is clearly not optimal for the sweep angle encountered here: the outside vane barely generates no-mixing, while the inside one operates at

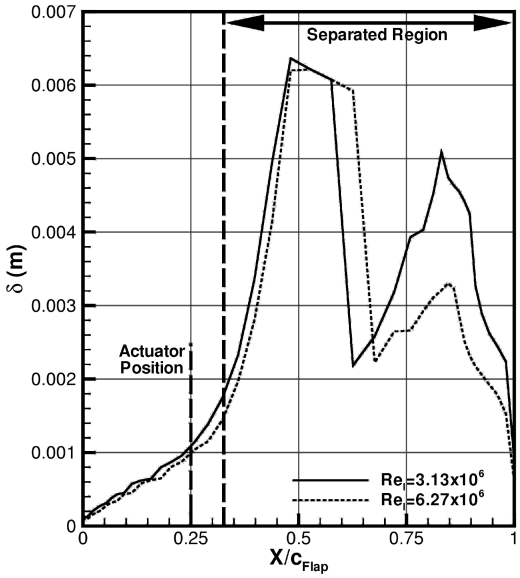

Fig. 9 Flap suction side boundary-layer thickness for the uncontrolled case.

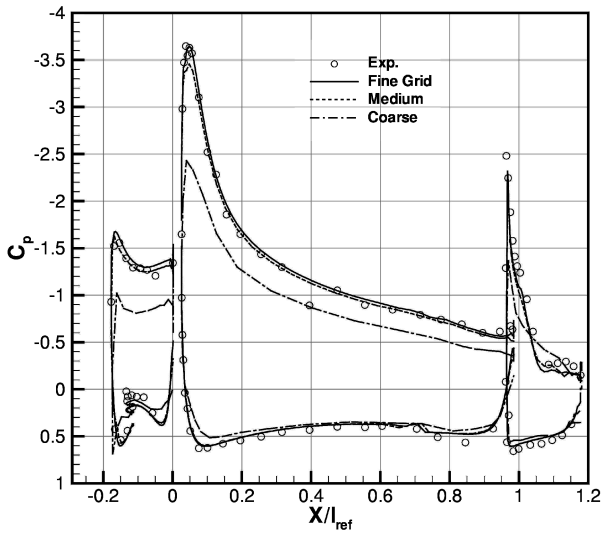

Fig. 8 Uncontrolled case, surface pressure distributions for the three levels of grid refinement.

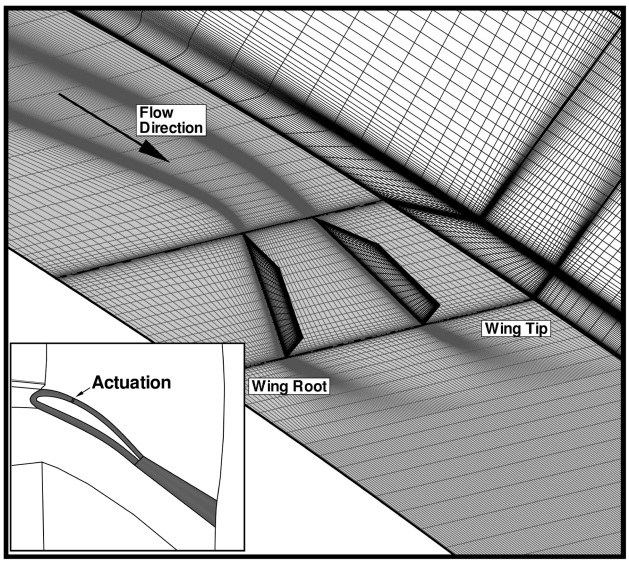

Fig. 10 Grid details for the case with SBVGs showing blocks with refined spanwise treatment.

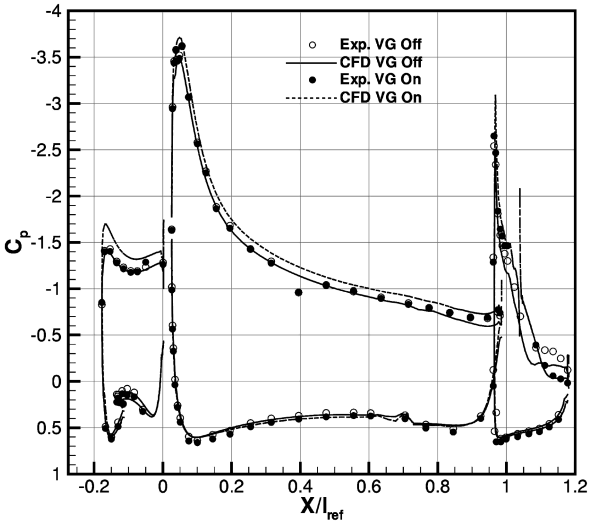

Fig. 11 Comparison of pressure distributions for the uncontrolled and SBVG-equipped cases.

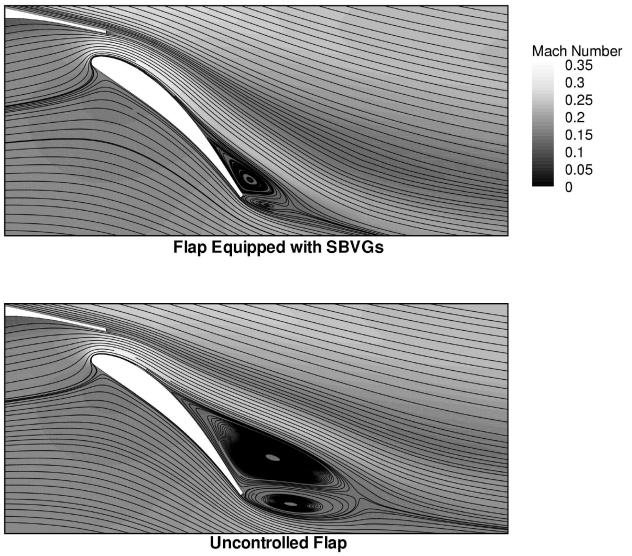

Fig. 12 Comparison of streamline patterns for the uncontrolled and SBVG-equipped cases.

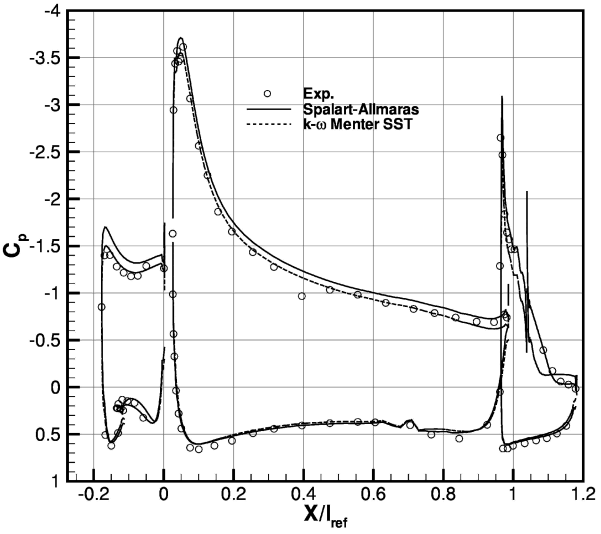

Fig. 14 Influence of turbulence modeling for the SBVG-equipped case.

near-stall conditions. In fact, corotating VGs perpendicular to the flap LE would probably have been a wiser choice for this type of configuration (as demonstrated during the AWIATOR program [5]).

Furthermore, from the contours of streamwise vorticity, the intensity of the longitudinal vortices is seen to decay relatively rapidly downstream of the actuators (total disappearance within 10–15 chords, i.e., 40–55 mm). In the absence of precise inflow measurements (with complex curvature effects adding on to that), it is difficult to isolate the origin of that rather fast diffusion. It could be a consequence of numerical dissipation, from too coarse a mesh being used, turbulence modeling inaccuracy, or even of purely physical effects given the strong adverse pressure gradients to be sustained.

3. *Influence of Turbulence Modeling*

When comparing the results obtained with SA's and Menter's SST k-ω models (for pressure distribution, Fig. 14, as well as lift coefficient, Table 3), we can see that the latter is far less accurate in predicting flow reattachment. This was not particularly expected because this formulation, designed to limit turbulent viscosity production in rotational regions, was especially derived for flows with well-established vortices, such as the ones met here. Yet, as

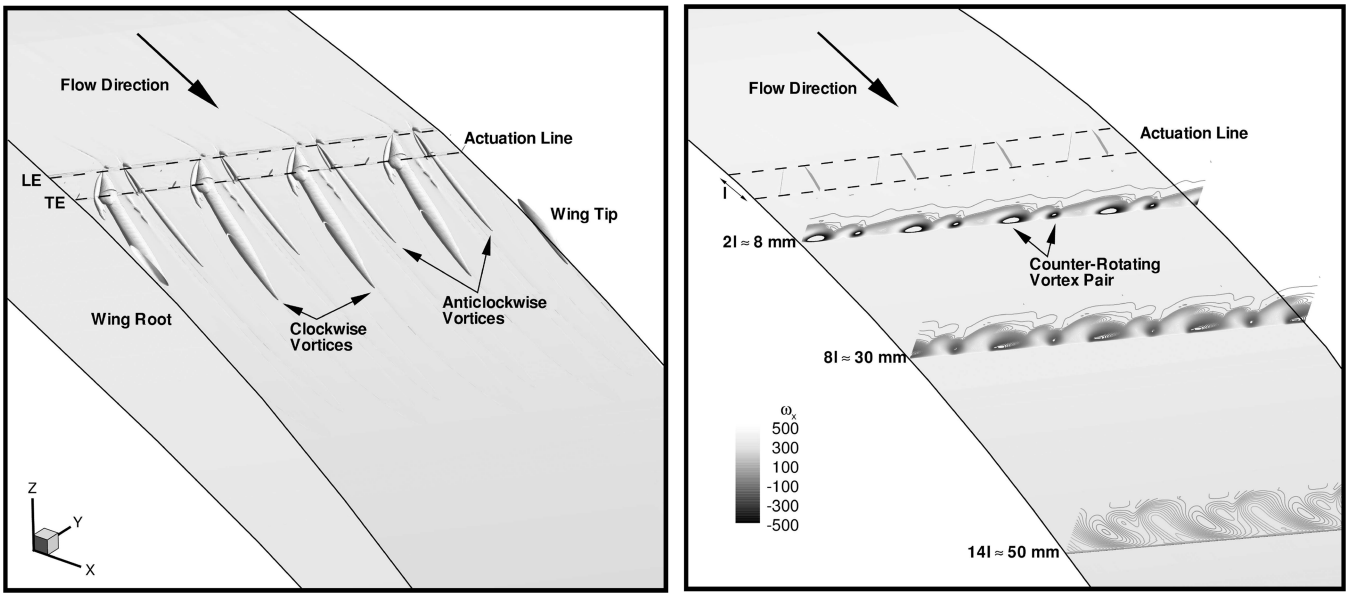

Fig. 13 Isosurface of positive Q criterion (left) and streamwise vorticity decay (right) for the SBVG-equipped case.

already shown during the uncontrolled case study, this model had a tendency to overpredict the extent of flap separation, placing the separation line too far upstream when compared with experimental results. This, in turn, would imply that the VGs are now located right inside the recirculation area and are therefore unable to produce the required mixing.

The inefficiency of the control scheme has an effect over the whole pressure pattern, with distributions over the slat and main element comparable in shape, accuracy, and values, to the uncontrolled experimental measurements. This, again, tends to demonstrate that the amplification of downwash at the flap trailing edge (TE) drives the entire airfoil circulation and should be accounted for through a reduction of the computational angle of attack.

4. *Reynolds Number and Incidence Effects*

As mechanical vane vortex generators are, by definition, passive and external means of achieving flow control, their dimensioning should be apprehended at multiple design points. It is a well-known fact that the efficiency of such devices is linked with local boundary thicknesses, which are known to be dependent on incidence and Reynolds number, among other parameters. Furthermore, the height of the system should be as limited as possible, so as to fit in the flap cove area when the flap is retracted and also to limit parasite drag. Only Spalart–Allmaras results will be discussed next.

Figure 15 shows that halving the freestream stagnation pressure to 1 bar ($Re_l = 3.13 \times 10^6$) does not have major effects on surface pressure distribution, with only a slightly decreased loading observed on each element. It is known already, from Fig. 9, that the change in Reynolds number has limited consequences on boundary-layer thickness at the actuator location, and we did not expect significant differences on the capacity of the control scheme to partially delay flap flow separation. Thus, it is not surprising that the pressure levels on the flap suction side are almost indistinguishable between the two results.

To quantify incidence effects, a computational angle of attack of 15 deg was chosen. This appeared high enough to be representative, while still giving attached flow on the main element [in fact, as incidence is increased, the extension of flap separation diminishes (from improved slot performance), up to $\alpha_{2.5D} \approx 22$ deg, where the flow is seen to be completely attached on the flap and large-scale vortices are shed from the main body].

From the close look at flap TE pressure levels in Fig. 16, the beneficial influences of improved boundary-layer homogenization are clearly visible again, with observations similar to these already drawn at 7 deg. Unfortunately, the absence of experimental results at that incidence did not allow for a more precise analysis of the case. Yet, from a strictly computational point of view (see also lift coefficient effects in Table 4), SBVGs can be considered as an efficient and robust means of controlling flow separation over wide ranges of flow conditions.

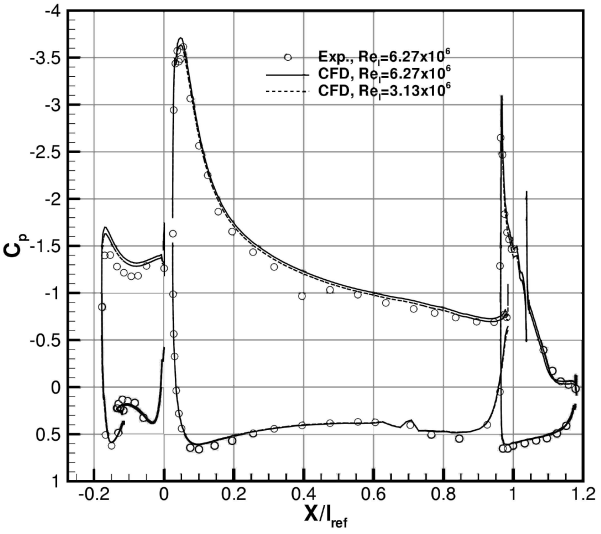

Fig. 15 Reynolds number effects for the SBVG-equipped case.

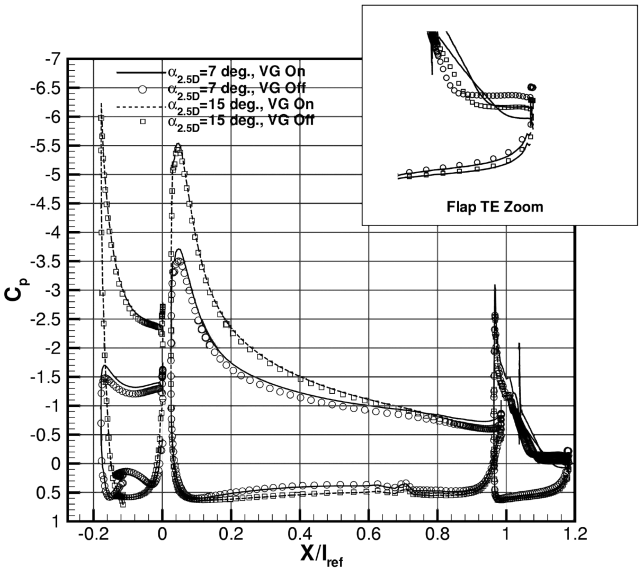

Fig. 16 Incidence effects for the SBVG-equipped case.

D. Three-Dimensional Results for the Wing Equipped with Sub-Boundary-Layer Vortex Generators

In the preceding paragraphs, we have seen that the current limitations to flow-control studies lie more in the cost of the computations themselves than the accuracy and prediction capability of Reynolds-averaged Navier–Stokes (RANS) modeling. This tends to limit the configurations to be assessed to very local (2.5-D in this case) subsets, which are not necessarily representative of "real" conditions and flow physics. A potential solution to that problem is discussed next and was applied to the three-dimensional evaluation of the complete AFV wing equipped with five pair of mechanical vortex generators.

1. *Source Term Modeling for Vane Vortex Generators*

An alternative to the use of costly body-conforming meshes is the simple description of VG effects using local source terms. These models allow for the simplification of mesh topologies and a nonnegligible reduction in the number of grid nodes. The model implemented in the elsA software is the one proposed by Bender et al. [49] and is based on a lifting-line theory. It was successfully applied

Table 3 Aerodynamic coefficients, turbulence modeling effects for the SBVG-equipped case

	C_l		L/D		ΔC_l	$\Delta(L/D)$
	Baseline	VGs	Baseline	VGs		
SA	1.6298	1.7427	28.5	33.2	+0.1129	+4.7
k-ω Menter SST	1.5595 ±0.03 (unsteady)	1.6178	26.6 ± 6	35.2	+0.0583	+8.6

Table 4 Aerodynamic coefficients, incidence effects for the SBVG-equipped case

	C_l		L/D		ΔC_l	$\Delta(L/D)$
	Baseline	VGs	Baseline	VGs		
$\alpha_{2.5D} = 7$ deg	1.6298	1.7427	28.5	33.2	+0.1129	+4.7
$\alpha_{2.5D} = 15$ deg	2.2248	2.2830	27.8	28.5	+0.0582	+0.7

by Jirásek [50] to a high-lift configuration at $M_\infty = 0.14$ and $Re_l = 1.65 \times 10^6$ and was deemed efficient for various design points, with a perfect agreement against experimental results. It simply consists in adding a source term to the momentum components of the RANS equations, that is, a specific force, based on the following formulation:

$$\mathbf{L}_i = C_{\mathrm{VG}} \cdot S_{\mathrm{VG}} \cdot \frac{\Delta V_i}{V_m} \cdot \rho \cdot (\mathbf{U} \cdot \mathbf{n}) \cdot (\mathbf{U} \cdot \mathbf{b}) \cdot \left(\frac{\mathbf{U} \cdot \mathbf{t}}{\|\mathbf{U}\|} \right) \quad (1)$$

In this expression, S_{VG} is the surface of the vane, ΔV_i and V_m are, respectively, the local (total) volume of the cell(s) forming the actuator, $(\mathbf{n}, \mathbf{b}, \mathbf{t})$ are the unit vectors describing the VG, and ρ and $\mathbf{U}$ are the density and velocity vector. C_{VG} is a user-defined constant parameter which, according to the literature [50], was set to a value of 10.

2. *Mesh Specifications*

Figure 17 provides an illustration of the three-dimensional mesh: it uses the same crossplane topology as the 2.5-D grid, extended over the entire 2-m-long span and 5 m further inside the fluid domain (from the wing tip). This time, the patched grid strategy was widely

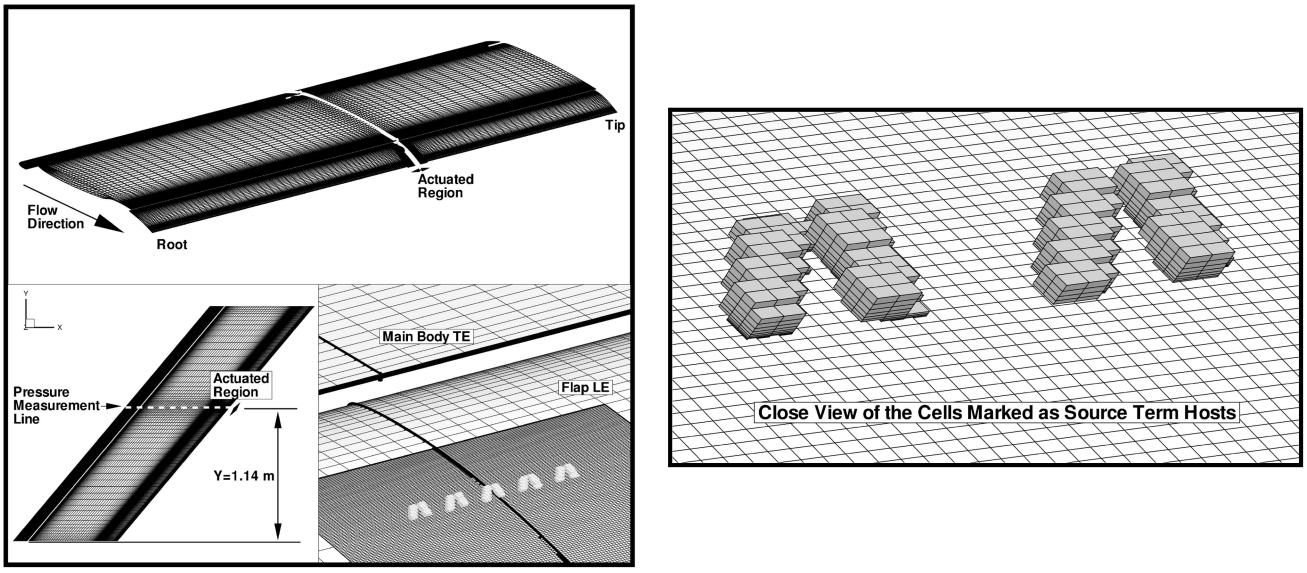

Fig. 17 Grid details for the complete 3-D AFV wing equipped with modeled SBVGs.

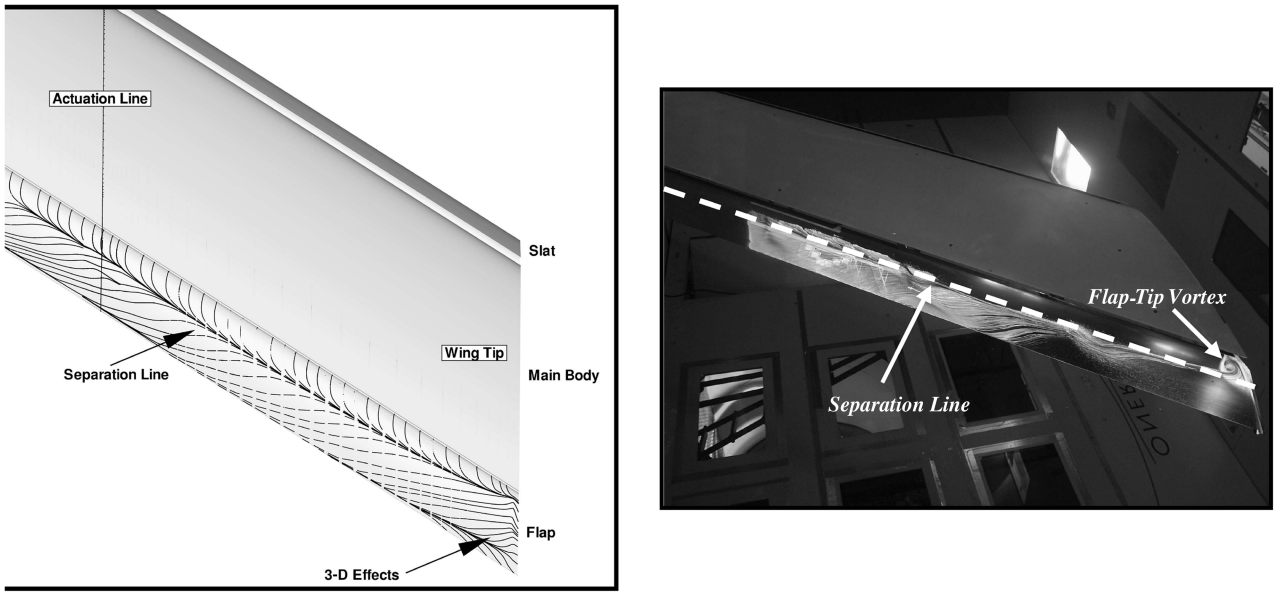

Fig. 18 Experimental ($\alpha = 19$ deg) and computational ($\alpha = 12$ deg) oil flow visualizations for the uncontrolled, 3-D cases.

extended, at various levels and in several directions, using different coarsening or refining ratios. Outside boundary layers, where the flow is known to be roughly bidimensional, the spanwise resolution was reduced, using a 1:2 ratio. In the flap region, and for the same blocks as those depicted in Fig. 10, the spanwise discretization was, on the other hand, refined (as initial computations showed that the original bunching did not properly capture separation outside the controlled region) with the same node-to-node proportion. Eventually, the two blocks where the VGs and their trails are to be located were gathered in an individual, much refined patch. This was done to ensure the following: first, the vanes would be modeled with a sufficient number of cells; second, that the spurious dissipation would remain limited for the longitudinal vortices to persist over realistic distances; third, that the cell size would be small enough to actually capture the vortices. The result is a mesh having 92 blocks and around 13×10^6 nodes, to be compared with the 2.5-D count of 9×10^6 points. From previous computations [46] on the AFV wing, a symmetry boundary condition was applied at the root plane. It is to be noted that, contrary to the experiment, a starboard half-wing was simulated.

3. Results

The flow conditions chosen for this part of the study are the same as previously stated, that is, an angle of attack of 12 deg at a Reynolds number of $Re_l = 6.27 \times 10^6$. Only results obtained with the Spalart–Allmaras model will be discussed.

The quality of the computational domain was first assessed with the source terms switched off, that is to say, without flow control. The experimental campaign started by applying the geometrical modifications of Fig. 4 to the original, fully instrumented flap, which allowed us to compare pressure distributions at various spanwise locations. The results, not reported here, showed that the agreement between the prediction and the experiment is very good indeed, except for a slight overestimation of suction level on the flap and an underestimation of velocity in the flap-separated region, which is commonly observed in RANS simulations of separated flow and quite comparable, in relative differences, to what has been reported until now. The location of the separation line is also seen to be well respected (Fig. 18). These combined points are thought to be indicative of a correct mesh quality, so that no grid modifications were applied for the controlled simulations.

Figure 19 shows pressure coefficient distributions when the source terms are turned back on, for the single measurement station available. Superimposed are results for the uncontrolled case at the same location. It is not surprising that the preceding comments on slat suction overshoot still apply for the controlled geometry. Indeed, the actuated area is quite limited in its spanwise extension (even more so than in the experimental run), so much so that the beneficial influence of local reattachment tends to be relatively limited, especially for swept configurations. A quick look at aerodynamic coefficients, Table 5, demonstrates that the gains to be expected are small compared to those of an infinite wing hypothesis, suggesting that, to be completely efficient, flow control should be applied over the entire spanwise separated region. As a matter of fact, experimental and computational results show that the slat and main-element loadings are not particularly increased, consistent with the remark on three-dimensional effects made during the 2.5-D review, where the infinite wing hypothesis simulated control over the complete span of the flap (a rather pronounced 40 deg sweep angle is known to introduce a strong curvature of near-boundary flow between the leading and trailing edges of the main element, likely to rapidly wash away all favorable influences of the limited extension of the controlled region). Only the main body is seen to benefit from local TE acceleration from improved LE suction on the flap. The action of the SBVGs is in very good agreement with experimental results, which demonstrates that the modeling strategy we applied is successful in generating average mixing tendencies having the right orders of magnitude.

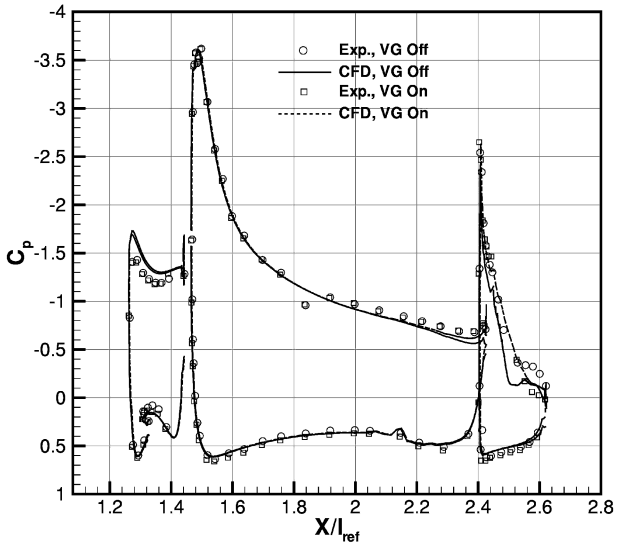

Fig. 19 Comparison of pressure distributions for the uncontrolled and SBVG-equipped 3-D cases.

Figure 20 presents a comparison of computed and observed skin-friction lines around the controlled region. Unfortunately, only $\alpha = 19$ deg pictures were acquired during the runs and will therefore be used as a reference. Both visualizations are very close to each other and the effects of sweep angle on oil flow deflection are well represented (note how control does not affect the left part of the figure). The separation line is seen to move significantly toward the flap TE under the influence of the streamwise vortices created by the vanes. Control authority is very local indeed and the original separation location recovered almost immediately. The plot of the vortical structures presented in Fig. 21 shows that the eddies generated by the outside vanes, which are known to be almost nonexistent, are not captured numerically, probably through a combined effect of limited modeling precision and strong numerical dissipation. The large-scale sheet is, on the other hand, well represented with a size and persistence similar to 2.5-D results.

E. Results for the Wing Equipped with Air-Jet Vortex Generators

1. Actuator Geometry and Mesh Specifications

The air-jet VGs employed during the test campaign were originally developed as pulsed jets by LPMO [44]. Unfortunately, several technical concerns did not allow for the actuators to be employed in their unsteady mode, and, as a result, only continuous blowing could be used throughout the entire tests. The actuator itself consists of a round jet exiting parallel to the flap leading edge, fed by a large rectangular cavity. Its dimensions, based on the notations of Fig. 22 and on the parameters introduced in Fig. 2, are restated in Table 6.

One of the advantages of active flow control is that the characteristics of the actuator can be quite easily adapted to varying specifications required either by the user or, in a more reactive fashion, by external physical inputs (say, local boundary-layer measurements for instance). The governing parameter chosen to pilot the jet exit flow is the ratio of jet to local velocity. Because of the lack of literature and knowledge on the topic, the most efficient experimental VR to be chosen during the tests was not known a priori for our particular case. A conservative choice was therefore made and a nominal ratio of VR = 2 was chosen, giving an average jet velocity of around 200 m/s

Table 5 Aerodynamic coefficients for the 3-D case equipped with SBVGs

	C_l	L/D	ΔC_l	$\Delta(L/D)$
VGs off	1.9806	7.2	+0.0157	0
VGs on	1.9963	7.2		

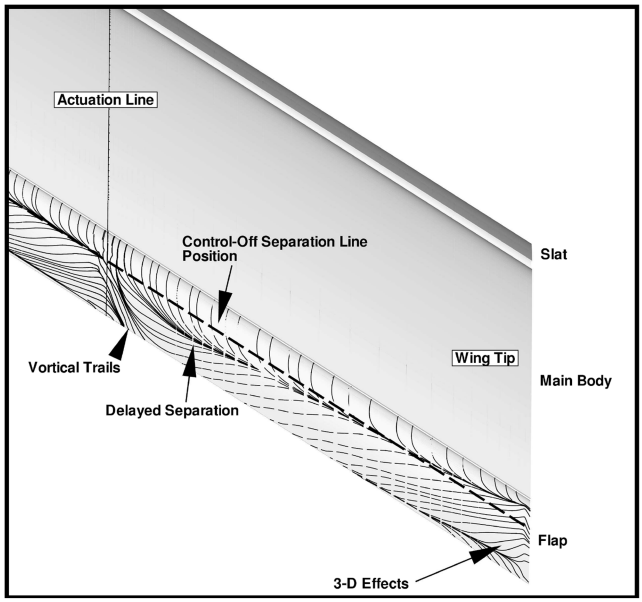

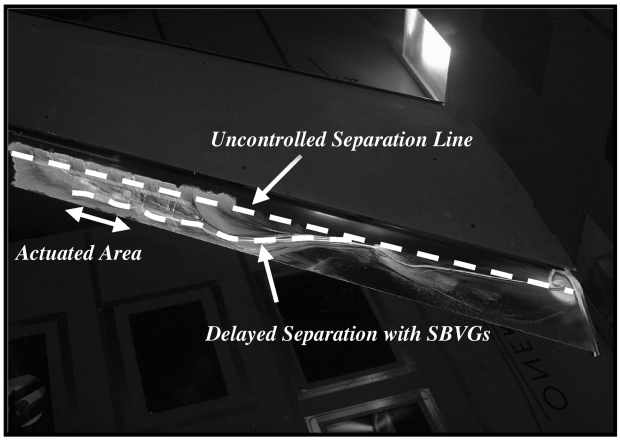

Fig. 20 Experimental ($\alpha = 19$ deg) and computational ($\alpha = 12$ deg) oil flow visualizations for the SBVG-equipped, 3-D cases.

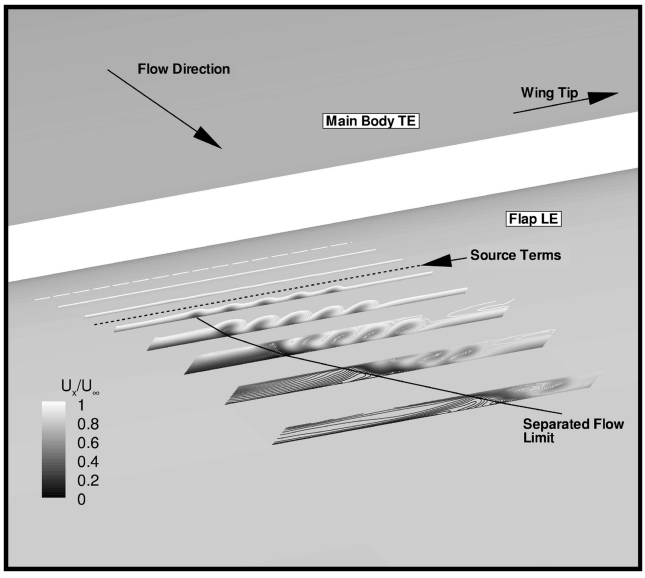

Fig. 21 Streamwise evolution of longitudinal velocity for the SBVG-equipped, 3-D case.

$$\left(C_\mu = \frac{\rho_j \cdot d_j \cdot \langle U_j \rangle^2}{\frac{1}{2} \cdot \rho_\infty \cdot l_{\text{ref}} \cdot U_\infty^2} = 0.86\%\right)$$

The Reynolds number for this test is set to $Re_l = 3.13 \times 10^6$ at $M_\infty = 0.22$.

A unique jet-cavity ensemble was simulated with a meshing strategy similar to that of the 2.5-D mechanical VGs. A mass-flow-type boundary condition was used to simulate fluid injection from the bottom surface of the cavity. Lateral faces are treated periodically assuming an infinite cavity length, which is realistic given the length-to-width ratio of the real actuator (set of 15 holes fed by the same cavity). Edge distributions around the hole and on the flap are based on previous experiences from jet-in-crossflow simulations and from the lessons learned with the mechanical VGs. The resulting computational domain displayed in Fig. 23 contains approximately 14.5×10^6 nodes after the application of the partially coincident joint strategy.

2. *Results*

Figure 24 illustrates a comparison of experimental and computational surface pressure coefficients for the wing equipped with air-jet (AJ) control. All the computations presented next were carried out using the Spalart–Allmaras turbulence model (the results already obtained with the vane VGs, for which the boundary-layer mixing physics is closely related to the one observed here, were believed to be good enough to justify that choice). No proper steady solution was reached for the finest grid level, with nicely periodic, limited oscillations from the remaining recirculation bubbles. This, in particular, explains the pressure overshoot observed around the flap TE. Furthermore, the relative cavity-orifice angle generates a very sharp turning angle and a massive separation inside the orifice itself, which limits the observed exiting average velocity to around 150 m/s (VR ≈ 1.5, $C_\mu = 0.48\%$) for the mass flow we imposed (instead of the 200 m/s we originally estimated).

The uncontrolled patterns have been commented on already and are only presented again for reference. Once again, the level of agreement between measurement and simulation is quite good indeed, with accurate pressure levels on the three elements. The phenomenon of increased suction discussed during the vane VGs survey is not as important with this configuration: the efficiency of the air jets in reattaching the boundary layer, although evident, seems

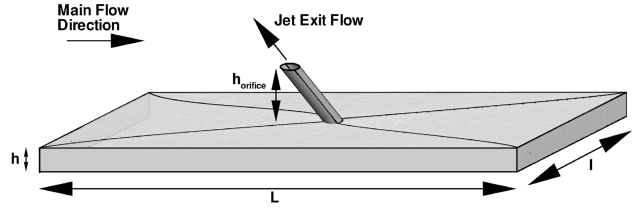

Fig. 22 Overview of the AJVG actuator geometry and defining parameters.

Table 6 Design parameters for the AJVGs

α	80 deg (blowing parallel to flap LE)
β	45 deg (toward wing root)
λ	4 mm
Φ	0.4 mm
L	10 mm
l	4 mm
h	0.5 mm
h_{orifice}	1.6 mm

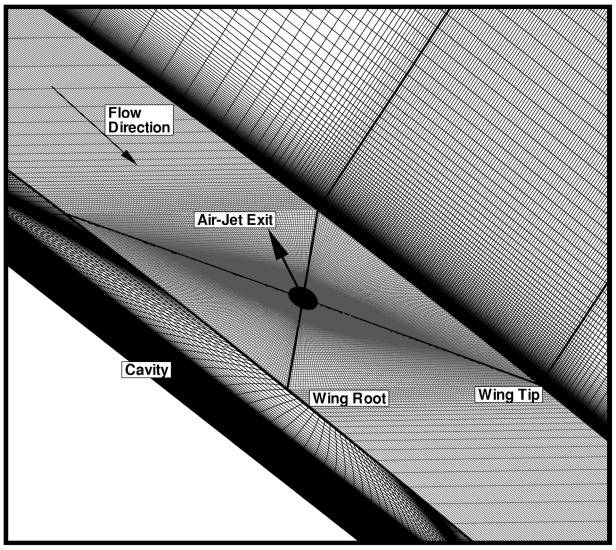

Fig. 23 Grid details for the case with AJVGs.

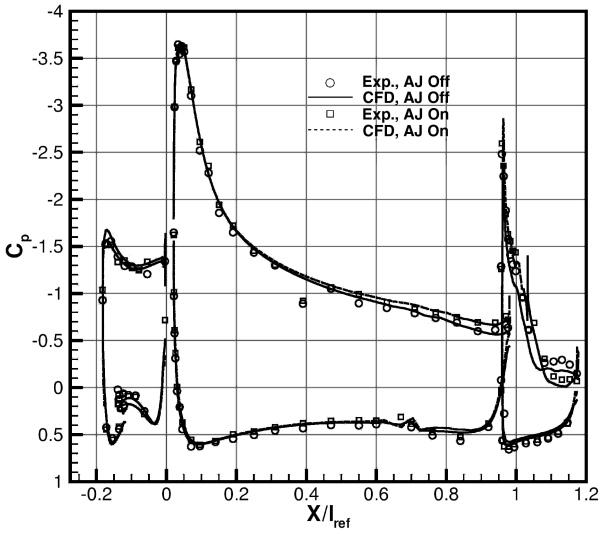

Fig. 24 Comparison of pressure distributions for the uncontrolled and AJ-equipped cases.

Table 7 Aerodynamic coefficients for the case equipped with *AJVGs*

	C_l	L/D	ΔC_l	$\Delta(L/D)$
VGs off	1.6298	28.5	+0.0617	+1.9
VGs on	1.6915	30.4		

a little less, so that the changes in overall circulation and induced incidence tend to be more limited.

A closer look at the flowfield generated by the jet exhaust in Fig. 25 shows vortical structures similar to these of classical, corotating, mechanical VGs, except for the horseshoe vortex development visible at the foot of the fluidic obstacle. When compared with Fig. 13, air jets are seen to produce much bigger and more intense streamwise vorticity cores, consistent with the observations made in our introduction. The decay rate, however, is about the same as that observed for the SBVG case, if not higher, which could explain the relative loss of efficiency of this device (see Table 7 for corresponding performances) compared with mechanical control.

V. Conclusions

This paper was interested in assessing steady RANS CFD methods and predictive capabilities for realistic flow-control problems under industrial conditions. Two types of actuating strategies, namely, sub-boundary-layer mechanical and air-jet vortex generators, were applied to the control of separation from the flap of a three-element, slotted airfoil, and computational results were compared with available experimental results from the AEROMEMS II European program. Overall, the agreement between numerical predictions and measurements was found to be very good indeed, with accurate surface pressure levels and correct responses to changes in freestream conditions.

However, the complexity of the problem and the number of physical scales involved has limited most of this study to 2.5-D test configurations which, although interesting, are not fully representative of real, in-flight conditions. To address that issue, a numerical model of a vane vortex generator, requiring minimal user input and meshing effort and allowing for multiple arrays to be simulated, was implemented in the elsA software and tested over a complete three-dimensional case. Results were seen to be very promising and computational costs were limited compared to similar studies using body-conforming meshes.

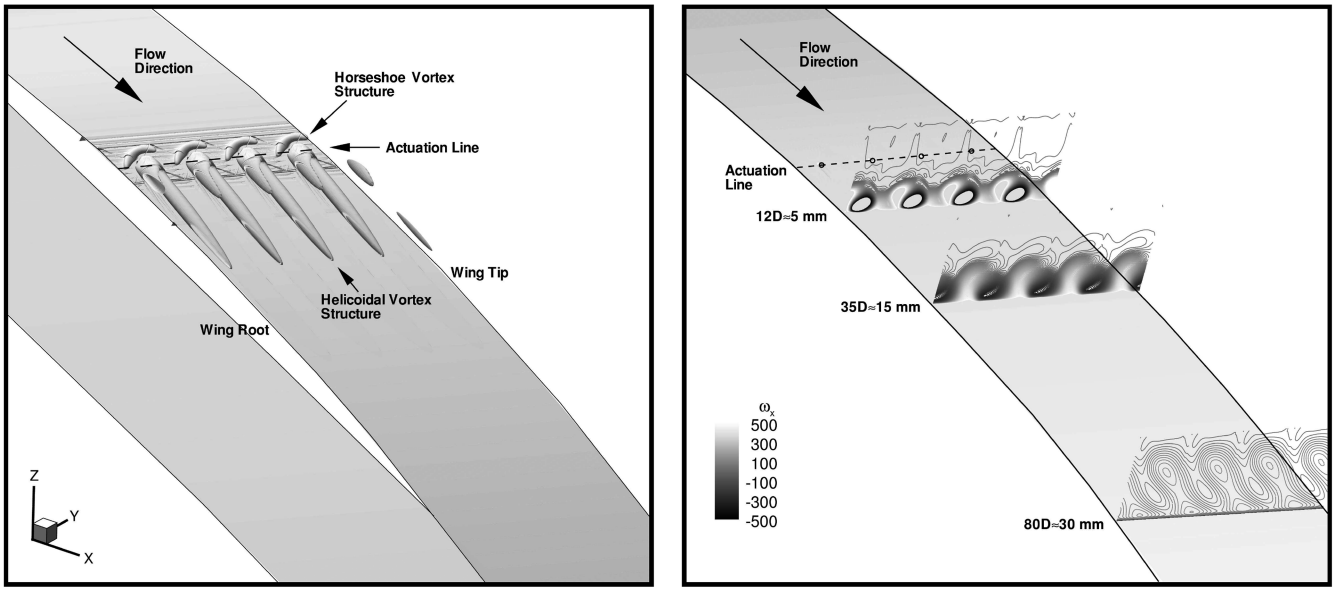

Fig. 25 Isosurface of positive Q criterion (left) and streamwise vorticity decay (right) for the AJ-equipped case.

Grid convergence and turbulence model dependency studies have proven that grid requirements for control problems are relatively severe but can be addressed using a multidirectional patched grid strategy. The simple one-equation formulation of Spalart and Allmaras [40] was seen to be capable of remarkable predictions, even for this kind of flow exhibiting complex interactions. With respect to the efficiency of flow control itself, the preceding results, and their experimental counterparts, indicate that there could be a lot to be gained from delaying flap separation, provided the actuated area is extended to the complete reverse flow region.

The whole problem of modern flow control lies in choosing and adapting the right actuator characteristics to each design point. To date, this has been done mainly empirically, or based on experimental considerations, which raises the question of maximum achievable control authority in an optimized environment. To tackle that problem, it would be interesting, for instance, to focus on applying optimization methods for the optimal positioning and parameterization of fluidic, periodic actuators on novel high-lift designs.

Acknowledgments

The work reported here is based on experimental results obtained by ONERA and Dassault Aviation in the scope of the Advanced Aerodynamic Flow Control Using Microelectromechanical Systems II European campaign (Contract No. G4RD-CT-2002-00748). This project is a collaboration between British Aerospace Systems, Dassault Aviation, Airbus Deutschland, GmbH, European Aeronautic Defence and Space Company Military Aircraft, Snecma, ONERA, DLR, Laboratoire de Physique et Metrologie des Oscillateurs, Manchester University, Laboratoire de Mécanique de Lille, Warwick University, Technical University of Berlin, Cranfield University, National Technical University of Athens, and Auxitrol. It was funded by the European Union and the project partners. The authors are particularly thankful to J.-P. Flodrops for his permanent availability and for supplying the wind-tunnel measurements. We are greatly indebted to J.-R. Frutos (Laboratoire de Physique et Metrologie des Oscillateurs) for his information on the air-jet actuator's development and design. We would also like to thank F. Moens for his expertise on high-lift aerodynamics, and P. Sagaut for his fruitful suggestions and comments throughout the completion of this study.

References

[1] Gad-el-Hak, M., *Flow Control: Passive, Active and Reactive Flow Management*, Cambridge Univ. Press, Cambridge, England, U.K., 2000.

[2] McLean, J. D., Crouch, J. D., Stoner, R. C., Sakurai, S., and Seidel, G. E., "Study of the Application of Separation Control by Unsteady Excitation to Civil Transport Aircraft," NASA Langley Research Center, NASA/CR-1999-209338, 1999.

[3] Nield, B. N., "An Overview of the Boeing 777 High Lift Aerodynamic Design," *The Aeronautical Journal*, Vol. 99, No. 989, 1995, pp. 361–371.

[4] Heinzen, S., Hall, C., and Chokani, N., "In-Flight Application of Active Separation Control Using Pulsed Jet Blowing," *40th AIAA Aerospace Sciences Meeting and Exhibit*, AIAA 2002-0416, Jan. 2002.

[5] Bohannon, K., "Passive Flow Control on Civil Aircraft Flaps Using Sub-Boundary Layer Vortex Generators in the AWIATOR Programme," *3rd AIAA Flow Control Conference*, AIAA 2006-2858, June 2006.

[6] Godard, G., and Stanislas, M. , "Control of a Decelerating Boundary Layer, Part 1: Optimization of Passive Vortex Generators," *Aerospace Science and Technology*, Vol. 10, No. 3, April 2006, pp. 181–191. doi:10.1016/j.ast.2005.11.007

[7] Lin, J. C., Robinson, S. K., McGhee, R. J., and Valarezo, W. O., "Separation Control on High-Lift Airfoils via Micro-Vortex Generators," *Journal of Aircraft*, Vol. 31, No. 6, Nov.–Dec. 1994, pp. 1317–1323. doi:10.2514/3.46653

[8] Lin, J. C., "Control of Turbulent Boundary Layer Separation Using Micro-Vortex Generators," *30th AIAA Fluid Dynamics Conference*, AIAA 1999-3404, 1999.

[9] Klausmeyer, S., Papadakis, M., and Lin, J., "A Flow Physics Study of Vortex Generators on a Multi-Element Airfoil," *34th AIAA Aerospace Sciences Meeting and Exhibit*, AIAA 1996-0548, Jan. 1996.

[10] Dodbele, S. S., Hobbs, C. R., Kern, S. B., Ghee, T. A., Hall, D. R., and Ely, W. L., "Wind Tunnel Experiments and Navier–Stokes Computations of a High-Lift Military Airfoil," *37th AIAA Aerospace Science Meeting and Exhibit*, AIAA 1999-0540, Jan. 1999.

[11] Rae, A. J., Galpin, S. A., Fulker, J., "Investigation into Scale Effects on the Performance of Sub Boundary-Layer Vortex Generators on Civil Aircraft High-Lift Devices, *1st AIAA Flow Control Conference*, AIAA 2002-3274, June 2002.

[12] Godard, G., and Stanislas, M. , "Control of a Decelerating Boundary Layer, Part 1: Optimization of Round Jets Vortex Generators," *Aerospace Science and Technology*, Vol. 10, No. 6, April 2006, pp. 455–464. doi:10.1016/j.ast.2005.11.005

[13] Wygnanski, I., "A Wind Tunnel Investigation of a Thin Airfoil with a Sharp Leading Edge and Blowing Applied at Mod-Chord at Two Angles Relative to the Surface," *Journal of the Royal Aeronautical Society*, Vol. 70, No. 666, 1966, p. 665.

[14] Innes, F., Pearcey, H. H., and Sykes, D. M., "Improvements in the Performance of a Three Element High Lift System by the Application of Airjet Vortex Generators," *The Aeronautical Journal*, Vol. 99, No. 987, 1995, pp. 265–274.

[15] Lindblad, I., and de Cock, K. M. J., "CFD Prediction of Maximum Lift for a 2D High Lift Configuration," *17th AIAA Applied Aerodynamics Conference*, AIAA No. 1999-3180, 1999.

[16] Lewington, N. P., Peake, D. J., Henry, F. S., and Singh, C., Analogue/Digital Wind Tunnel Testing of Active Low Momentum Flow Control on Single and Multi-Component Airfoil Systems at High Lift," *40th AIAA Aerospace Sciences Meeting and Exhibit*, AIAA 2002-0303, Jan. 2002.

[17] Lewington, N. P., "Enhancing Lift on a Three-Element High Lift Aerofoil System by Installing Air-Jet Vortex Generators," Ph.D. Thesis, London City Univ., London, Nov. 2001.

[18] Warsop, C., "Results and Lessons Learned from the European AEROMEMS II Project," *3rd AIAA Flow Control Conference*, AIAA 2006-3503, June 2006.

[19] Crowther, W. J., "Control of Separation on a Trailing Edge Flap Using Air Jet Vortex Generators," *Journal of Aircraft*, Vol. 43, No. 5, 2006, pp. 1589–1593. doi:10.2514/1.15755

[20] Glezer, A., and Amitay, M., "Synthetic Jets," *Annual Review of Fluid Mechanics*, Vol. 34, Jan. 2002, pp. 503–529. doi:10.1146/annurev.fluid.34.090501.094913

[21] Oster, D., Wygnanski, I., Dziomba, B., and Fiedler, H., *On the Effect of Initial Conditions on the Two-Dimensional, Turbulent Mixing Layer*, Structure and Mechanics of Turbulence 1, Vol. 75, Springer–Verlag, Berlin, 1978, pp. 48–64.

[22] Seifert, A., Bachar, T., Koss, D., Shepshelovich, M., and Wygnanski, I., "Oscillatory Blowing: A Tool to Delay Boundary Layer Separation," *AIAA Journal*, Vol. 31, No. 11, Nov. 1993, pp. 2052–2060. doi:10.2514/3.49121

[23] Seifert, A., Darabi, A., and Wygnanski, I., "Delay of Airfoil Stall by Periodic Excitation," *Journal of Aircraft*, Vol. 33, No. 4, July–Aug. 1996, pp. 691–698. doi:10.2514/3.47003

[24] Seifert, A., and Pack, L. G., "Oscillatory Control of Separation at High Reynolds Numbers," *AIAA Journal*, Vol. 37, No. 9, Sept. 1999, pp. 1062–1071. doi:10.2514/2.834

[25] Nishri, B., and Wygnanski, I., "Effects of Periodic Excitation on Turbulent Flow Separation from a Flap," *AIAA Journal*, Vol. 36, No. 4, April 1998, pp. 547–556. doi:10.2514/2.428

[26] Tinapp, F., and Nitsche, W., "LDV-Measurements on a High-Lift Configuration with Separation Control," *Selected Papers from the 9th International Symposium on Applications of Laser Techniques to Fluid Mechanics*, Springer–Verlag, Berlin, 1998, pp. 19.1–19.8.

[27] Tinapp, F., and Nitsche, W., "On Active Control of High-Lift Flow," *Engineering Turbulence Modelling and Experiments 4: Proceedings of the 4th International Symposium on Engineering Turbulence Modelling and Measurements*, Elsevier, New York, 1999, pp. 619–626.

[28] Petz, R., and Nitsche, W., "Active Separation Control on a High-Lift Configuration by a Periodically Pulsating Jet," *24th International Congress of the Aeronautical Sciences (ICAS)*, International Council of the Aeronautical Sciences Paper 2004-118, 2004.

[29] Petz, R., and Nitsche, W., "Active Control of Flow Separation on a Swept Constant Chord Model in a High-Lift Configuration," *3rd AIAA*

Flow Control Conference, AIAA 2006-3505, 2006.

[30] Schatz, M., Thiele, F., Petz, R., and Nitsche, W., "Separation Control by Periodic Excitation and its Application to a High Lift Configuration," *2nd AIAA Flow Control Conference*, AIAA 2004-2507, 2004.

[31] Greenblatt, D., "Dual Location Separation Control on a Semi-Span Wing," *23rd AIAA Applied Aerodynamics Conference*, AIAA 2005-5085, 2005.

[32] Nagib, H., Kiedaisch, J., Reinhard, P., and Demanett, B., "Control Techniques for Flows with Large Separated Regions: A New Look at Scaling Parameters," *3rd AIAA Flow Control Conference*, AIAA 2006-2857, 2006.

[33] Pack Melton, L., Schaeffler, N. W., Yao, C.-S., and Seifert, A., "Active Control of Flow Separation from Supercritical Airfoil Leading-Edge Flap Shoulder," *Journal of Aircraft*, Vol. 42, No. 5, 2005, pp. 1142–1149.
doi:10.2514/1.10294

[34] Pack Melton, L., Yao, C.-S., and Seifert, A., "Active Control of Separation from the Flap of a Supercritical Airfoil," *33rd AIAA Fluid Dynamics Conference and Exhibit*, AIAA 2003-4005, 2003.

[35] Pack Melton, L., Yao, C.-S., and Seifert, A., "Application of Excitation from Multiple Locations on a Simplified High-Lift System," *2nd AIAA Flow Control Conference*, AIAA 2004-2324, 2004.

[36] Kiedaisch, J., Nagib, H., and Demanett, B., "Active Flow Control Applied to High-Lift Airfoils Utilizing Simple Flaps," *3rd AIAA Flow Control Conference*, AIAA 2006-2856, 2006.

[37] Becker, R., King, R., Petz, R., and Nitsche, W., "Adaptative Closed-Loop Separation Control on a High-Lift Configuration Using Extremum Seeking," *AIAA Journal*, Vol. 45, No. 6, 2007, pp. 1382–1392.
doi:10.2514/1.24941

[38] Cambier, L., and Gazaix, M., "elsA: An Efficient Object-Oriented Solution to CFD Complexity," *40th AIAA Aerospace Sciences Meeting and Exhibit*, AIAA 2002-0108, Jan. 2002, http://elsa.onera.fr.

[39] Cambier, L., and Veuillot, J.-P., "Status of the elsA CFD Software for Flow Simulation and Multidisciplinary Applications," *46th AIAA Aerospace Sciences Meeting and Exhibit*, AIAA 2008-0664, Jan. 2008.

[40] Spalart, P. and Allmaras, S., "A One Equation Turbulence Model for Aerodynamic Flows," *La Recherche Aérospatiale*, Vol. 1, No. 5, 1994, pp. 5–21.

[41] Menter, R., "Two-Equation Eddy-Viscosity Turbulence Model for Engineering Applications," *AIAA Journal*, Vol. 32, No. 8, 1994, pp. 1598–1605.
doi:10.2514/3.12149

[42] Flodrops, J.-P., "Flap Flow Separation Control for a High-Lift Swept Wing in the ONERA F1 Industrial Wind Tunnel," ONERA RF 1/07108 DAAP, Sept. 2005.

[43] Hansen, H., Thiede, P., Moens, F., Rudnik, R., and Quest, J., "Overview About the European High Lift Research Project EUROLIFT," *42nd AIAA Aerospace Sciences Meeting and Exhibit*, AIAA 2004-0767, 2004.

[44] Frutos, J. R., Vernier, D., Bastien, F., de Labachelerie, M., and Bailly, Y., "An Electrostatically Actuated Valve for Turbulent Boundary Layer Control," *Sensors 2005 IEEE Conference*, Inst. of Electrical and Electronics Engineers, New York, 2005.

[45] Brunet, V., Francois, C., Garnier, E., and Pruvost, M., "Experimental and Numerical Investigations of Vortex Generators Effects," *3rd AIAA Flow Control Conference*, AIAA 2006-3027, 2006.

[46] Moens, F., "ONERA-RANS Activities Carried Out for Eurolift, W. P.2.1," ONERA RT 81/03631 DAAP, Feb. 2003.

[47] Roache, P. J., "Verification and Validation in Computational Science and Engineering," Hermosa Publishers, Albuquerque, NM, 1998; See also http://www.grc.nasa.gov/WWW/wind/valid/tutorial/tutorial.html

[48] Esquieu, S., "Evaluation de la Traînée d'un Avion de Transport à Partir de Calculs Numériques de Mécanique des Fluides (Civil Aircraft Drag Extraction from CFD Results)," Ph.D. Thesis, Bordeaux 1/ONERA, Bordeaux, France, Dec. 2003.

[49] Bender, E. E., Anderson, B. H., and Yagle, P. J., "Vortex Generator Modelling for Navier-Stokes Codes," *Fluids Engineering Division Summer Meeting* FED 99-6919, July 1999.

[50] Jirásek, A., "A Vortex Generator Model and its Application to Flow Control," *Journal of Aircraft*, Vol. 42, No. 6, 2005, pp. 1486–1491.
doi:10.2514/1.12220